

Kinematic and dynamical origins of mean- p_T fluctuations in heavy-ion collisions

Lipei Du^{a,b}

^a*Department of Physics, University of California, Berkeley, 94270, CA, USA*

^b*Nuclear Science Division, Lawrence Berkeley National Laboratory, Berkeley, 94270, CA, USA*

Abstract

Event-by-event fluctuations of the mean transverse momentum (mean- p_T) provide a sensitive probe of collective dynamics beyond single-particle spectra and anisotropic flow. In this Letter, we present a systematic comparison of mean- p_T fluctuation measurements with calculations based on a Bayesian-calibrated multistage hydrodynamic framework. The experimental definitions employed by the STAR and ALICE Collaborations are implemented explicitly and found to yield consistent results within controlled limits. We study the centrality and beam-energy dependence of the observable, its sensitivity to key soft-sector ingredients, and the impact of the kinematic p_T acceptance. By introducing scaled- p_T cuts, we demonstrate that a part of the apparent energy dependence arises from kinematic projection effects, while the remaining trends reflect genuine collective dynamics. Our results establish mean- p_T fluctuations as a nontrivial and independent validation of calibrated hydrodynamic descriptions of the quark-gluon plasma.

Keywords: transverse-momentum fluctuations, event-by-event correlations, relativistic heavy-ion collisions, multistage hydrodynamic models, kinematic acceptance effects

1. Introduction

Relativistic heavy-ion collisions produce strongly interacting matter that exhibits pronounced collective behavior, commonly described as the hydrodynamic expansion of a quark-gluon plasma (QGP) [1, 2]. Extensive experimental and theoretical studies have shown that single-particle spectra and anisotropic flow coefficients provide stringent constraints on the bulk properties and transport coefficients of the medium [3–9]. Event-by-event fluctuations offer complementary information by probing the response of the system to initial-state inhomogeneities and dynamical fluctuations that are not accessible through event-averaged observables [10, 11].

Fluctuations of the event-wise mean transverse momentum are among the most interesting event-by-event observables. Experimental measurements have revealed characteristic centrality and beam-energy systematics, including an overall dilution of fluctuations with increasing system size and a nontrivial evolution from RHIC to LHC energies [12–17]. These trends have been discussed in terms of partial thermalization, the number of effective particle-emitting sources, and the growth of collective radial expansion [11, 18–20]. Despite this long history, a quantitative interpretation of mean- p_T fluctuations within a modern, globally calibrated multistage hydrodynamic framework has remained limited.

Recent progress in Bayesian parameter estimation [21] has enabled the systematic calibration of multistage hydrodynamic models to a broad set of soft-sector observables, including particle yields, transverse-momentum spectra, and anisotropic flow

coefficients [5–9]. Such calibrations provide a controlled baseline for confronting additional observables that were not included in the fitting procedure. Mean- p_T fluctuations are particularly well suited for this purpose, as they are sensitive to event-by-event variations of radial flow, freeze-out conditions, and late-stage hadronic dynamics, while being only weakly constrained by the observables typically used in the calibration.

An additional challenge in interpreting existing measurements is that different experiments employ distinct definitions and weighting procedures for mean- p_T fluctuation observables. In particular, the prescriptions used by the STAR and ALICE Collaborations differ in their treatment of particle pairs, multiplicity weighting, and kinematic acceptance [14–16]. A meaningful model–data comparison therefore requires an explicit implementation of the experimental definitions, rather than relying on a single idealized observable.

In this Letter, we present a systematic comparison of mean- p_T fluctuation measurements with predictions from a Bayesian-calibrated multistage hydrodynamic model at top RHIC and LHC energies [8, 9]. We implement the STAR and ALICE definitions explicitly, examine the centrality and beam-energy dependence of the observable, and study its sensitivity to key soft-sector model ingredients. We further investigate the role of the kinematic p_T acceptance by comparing results obtained with experimental and scaled p_T cuts, allowing us to disentangle genuine dynamical trends from kinematic projection effects.

The remainder of this Letter is organized as follows. Section 2 describes the hydrodynamic framework and the analysis setup, including the implementation of the experimental definitions of the transverse-momentum fluctuation observable. Section 3 presents the main results, focusing on the centrality and

Email address: 1du2@lbl.gov (Lipei Du)

beam-energy dependence of mean- p_T fluctuations, their sensitivity to key model ingredients, and the role of kinematic acceptance effects. Finally, Section 4 summarizes the main findings and outlines implications for future fluctuation measurements.

2. Model and analysis setup

2.1. Bayesian-calibrated multistage hydrodynamic framework

The model calculations presented in this work are based on the same Bayesian-calibrated multistage hydrodynamic framework [8, 9, 22] employed in our recent study of transverse-momentum-differential radial flow fluctuations, $v_0(p_T)$ [23]. Here we summarize only the essential ingredients relevant for the present analysis of mean- p_T fluctuations and refer the reader to Refs. [8, 9, 22, 23] for a comprehensive description and validation.

The simulations are performed within the JETSCAPE framework (v3.7) [24] using a TRENTO-based initial condition model [25], followed by a short period of pre-equilibrium free streaming [26, 27] and subsequent second-order viscous hydrodynamic evolution with MUSIC [28–30]. The hydrodynamic stage includes temperature-dependent shear and bulk viscosities constrained by Bayesian inference to a broad set of soft-sector observables at both RHIC and LHC energies [8, 9, 22]. Hadronization is implemented via Cooper–Frye sampling at a switching temperature T_{sw} [31], with viscous corrections to the distribution function [32, 33], and the subsequent hadronic rescattering stage is modeled using the SMASH transport code [34].

In the present work, we use the Maximum A Posteriori (MAP) parameter set from the Bayesian analysis [8, 9, 22] as a fixed baseline and perform forward model calculations without retuning. This setup provides a predictive test of the calibrated framework at $\sqrt{s_{NN}} = 200$ GeV and 5.02 TeV, since the mean- p_T fluctuation observables at these energies were not included in the original calibration, while the corresponding data at $\sqrt{s_{NN}} = 2.76$ TeV were [8, 9]. Variations around this baseline [23]—such as switching off bulk viscosity, removing the hadronic afterburner, modifying the nucleon size in the initial conditions, or considering ideal hydrodynamic evolution—are used to assess the sensitivity of the observable to different stages of the collision dynamics.

2.2. Definition of the transverse-momentum fluctuation observable

The observable studied in this work is an event-by-event measure of correlated transverse-momentum fluctuations, designed to quantify dynamical fluctuations beyond trivial statistical sampling. Unlike single-particle spectra or average flow coefficients, this observable probes correlations between particles within the same event and is therefore sensitive to event-wise fluctuations of collective radial expansion, freeze-out conditions, and late-stage dynamics.

At the core of the analysis is the two-particle transverse-momentum covariance C_m , evaluated for particles within a

given kinematic acceptance and centrality class. For a single event containing N particles, the covariance is defined as [35, 36]

$$C_m^{(\text{event})} = \frac{1}{N(N-1)} \sum_{i \neq j} (p_{T,i} - p_{T,\text{ref}})(p_{T,j} - p_{T,\text{ref}}), \quad (1)$$

where $p_{T,i}$ denotes the transverse momentum of particle i and $p_{T,\text{ref}}$ is a reference mean transverse momentum. The precise definition of this reference mean distinguishes the experimental prescriptions used by different collaborations, as discussed below.

The experimentally reported quantity is obtained by averaging the event-wise covariance over all events within a given centrality bin, $C_m = \langle C_m^{(\text{event})} \rangle_{\text{events}}$, and normalizing it by the squared mean transverse momentum. Specifically, we define the dimensionless fluctuation measure

$$R_{p_T} \equiv \sqrt{C_m} / \langle p_T \rangle,$$

where $\langle p_T \rangle \equiv \langle [p_T] \rangle$ denotes the ensemble-averaged mean transverse momentum in the same centrality class and acceptance. This normalization removes trivial scaling with the absolute momentum scale and enables meaningful comparisons across centrality, beam energy, and particle species.¹

Physically, R_{p_T} quantifies the relative magnitude of correlated momentum fluctuations within an event. Event-by-event variations of the collective transverse velocity field lead to coherent shifts of particle momenta, generating positive two-particle covariances that survive the averaging over events. As a result, R_{p_T} is particularly sensitive to fluctuations of radial collectivity and to mechanisms that amplify or damp such fluctuations, including viscous effects, initial-state granularity, and hadronic rescattering.

2.3. Implementation of experimental definitions

In this work, we explicitly implement the transverse-momentum fluctuation definitions used by the STAR and ALICE Collaborations at the particle level, applying identical kinematic cuts to the model and the data [14–16]. The two prescriptions differ in the choice of the reference mean $p_{T,\text{ref}}$ appearing in Eq. (1). In the STAR definition, $p_{T,\text{ref}}$ is taken to be the ensemble-averaged mean transverse momentum within a given centrality class, $p_{T,\text{ref}}^{\text{STAR}} = \langle [p_T] \rangle_{\text{events}}$, where $[p_T]$ is the event-wise mean transverse momentum. In contrast, the ALICE prescription uses the event-wise mean itself as the reference, $p_{T,\text{ref}}^{\text{ALICE}} = [p_T]^{(\text{event})}$.

As shown analytically in Appendix A, the STAR observable can be decomposed into the ALICE-style two-particle covariance plus an additional term proportional to the variance of the event-wise mean transverse momentum, $\langle (|p_T|_i - \langle p_T \rangle)^2 \rangle$. The magnitude of this additional contribution depends on particle multiplicity and the width of the centrality bin, and may in principle lead to quantitative differences between the two definitions.

¹Residual kinematic effects associated with the finite p_T acceptance can still influence such comparisons, as discussed in Sec. 3.

3. Results and discussion

3.1. Baseline comparison and sensitivity to soft kinematics

We begin with a baseline comparison of $\sqrt{C_m}/\langle p_T \rangle$ at $\sqrt{s_{NN}} = 200$ GeV, shown in Fig. 1, where model calculations are confronted with STAR measurements as a function of centrality [14]. The results are evaluated using the experimental kinematic acceptance $0.2 < p_T < 2$ GeV as in the data. Applying both the STAR and ALICE fluctuation definitions to the same set of model events with identical kinematic cuts, we find that the two prescriptions yield numerically indistinguishable results across all centralities considered. This confirms that, for the large multiplicities and narrow centrality bins employed here, the additional variance term discussed in Appendix A is subleading. In view of this near-equivalence, only the STAR-style result is shown in Fig. 1.

While the STAR- and ALICE-style model evaluations are mutually consistent, the model systematically underestimates the measured fluctuation magnitude when the experimental lower p_T cut of 0.2 GeV is used. A similar underestimation is observed in the Bayesian inference study at $\sqrt{s_{NN}} = 2.76$ TeV, where mean- p_T fluctuation data were included in the calibration, yet the MAP parameter set nevertheless yields systematically smaller fluctuation magnitudes for the experimental acceptance [9]. This indicates that the trend observed at 200 GeV reflects a systematic feature of the calibrated framework rather than an isolated discrepancy. To investigate the origin of this difference, we varied the lower edge of the acceptance window within the model while keeping the upper cut fixed. As illustrated in Fig. 1, lowering p_T^{\min} leads to a noticeable increase of $\sqrt{C_m}/\langle p_T \rangle$ and improves the agreement with the data.

This sensitivity to the lower p_T cut indicates that the p_T -integrated fluctuation observable is dominated by correlations carried by the very soft part of the spectrum, where collective radial dynamics are most pronounced. Schematically, the event-averaged covariance can be written as

$$C_m \sim \int dp_T dp'_T \frac{dN}{dp_T} \frac{dN}{dp'_T} \langle \delta p_T \delta p'_T \rangle, \quad (2)$$

illustrating that the dominant contribution arises from the low- p_T region where particle yields (dN/dp_T) are largest and momentum shifts induced by collective flow fluctuations are coherent (see also Appendix B). The residual discrepancy between the model and the data for the nominal experimental cuts therefore suggests that, within the present setup, the strength of event-by-event radial collectivity in the soft sector may be slightly underestimated. Crucially, the near-identical results obtained using the STAR and ALICE definitions demonstrate that this conclusion is robust with respect to reasonable variations in the fluctuation definition and is not an artifact of the averaging procedure.

These observations motivate the more systematic investigation of kinematic acceptance effects presented in the following sections, where we examine how the projection of momentum correlations onto different p_T windows influences comparisons across beam energies and particle species.

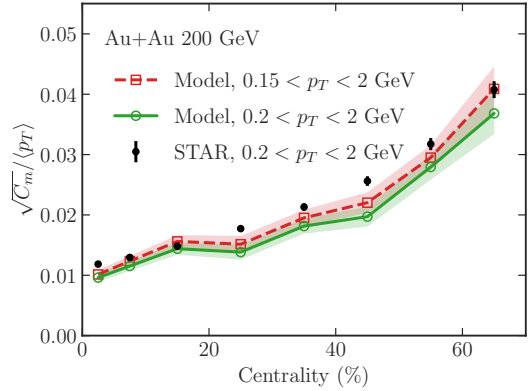


Figure 1: Centrality dependence of $\sqrt{C_m}/\langle p_T \rangle$ in Au+Au collisions at $\sqrt{s_{NN}} = 200$ GeV. Model calculations are shown for two different lower transverse-momentum cuts, $0.15 < p_T < 2$ GeV and $0.2 < p_T < 2$ GeV, illustrating the sensitivity of the integrated observable to the kinematic acceptance. Published STAR data for $0.2 < p_T < 2$ GeV are shown for comparison [14].

3.2. Sensitivity to model ingredients at fixed beam energy

We next examine how $R_{p_T} \equiv \sqrt{C_m}/\langle p_T \rangle$ responds to variations of key model ingredients, focusing on Au+Au collisions at $\sqrt{s_{NN}} = 200$ GeV. The results are summarized in Fig. 2, where the relative change of R_{p_T} is shown with respect to a common baseline setup corresponding to the Bayesian-calibrated reference model [8, 9], which includes shear and bulk viscosity, finite nucleon size ($w = 1.12$ fm), and a hadronic afterburner. To emphasize the intrinsic sensitivity of the observable, all results are presented as fractional deviations from this baseline.

Two representative centrality classes, 30–40% and 50–60%, are shown. This choice allows us to contrast a mid-central regime, where collective dynamics are well developed, with a more peripheral regime, where multiplicities are smaller and different fluctuation sources compete more strongly. As illustrated in Fig. 2, the response of R_{p_T} to individual model modifications is clearly centrality dependent and does not follow a universal ordering across all variants.

Turning off bulk viscosity (“no bulk”) leads to a small change in R_{p_T} , with a slightly negative response in 30–40% collisions and a positive response in the more peripheral 50–60% class. This pattern suggests that bulk-viscous effects contribute more visibly to transverse-momentum fluctuations in dilute systems, where bulk-pressure variations are less efficiently damped. However, the overall magnitude of the response is modest in both centrality classes. Since turning off bulk viscosity hardens the single-particle spectra, it simultaneously enhances the correlated covariance sampled within the fixed p_T window while increasing the mean transverse momentum in the denominator, leading to a partial cancellation in the normalized ratio R_{p_T} .

In contrast, the ideal-hydrodynamic limit (“ideal hydro”), in which shear viscosity is also switched off and viscous damping is absent, produces a systematic enhancement of R_{p_T} in both centrality classes, with a larger relative effect in 50–60% collisions. This behavior is consistent with the interpretation of R_{p_T} as a genuine fluctuation observable that is sensitive to dissipa-

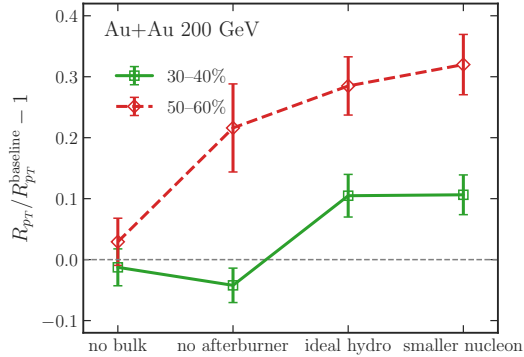


Figure 2: Relative response of $R_{pT} \equiv \sqrt{C_m}/\langle p_T \rangle$ to variations of model ingredients in Au+Au collisions at $\sqrt{s_{NN}} = 200$ GeV. Results are shown as fractional deviations with respect to the baseline calculation that includes shear and bulk viscosity, finite nucleon size, and a hadronic afterburner. Two representative centrality classes, 30–40% and 50–60%, are shown. The model variants correspond to switching off bulk viscosity (“no bulk”), disabling the hadronic afterburner (“no afterburner”), ideal hydrodynamic evolution without viscosity (“ideal hydro”), and a reduced nucleon size (“smaller nucleon”). Error bars indicate statistical uncertainties from the finite event sample.

tive smoothing of event-by-event radial expansion. A comparison of the “no bulk” and “ideal hydro” cases shows that R_{pT} responds more strongly to the removal of shear viscosity than to bulk viscosity within the present setup, indicating that shear-driven damping of transverse velocity gradients plays a dominant role in suppressing correlated momentum fluctuations.

This sensitivity pattern contrasts with that of the p_T -differential radial-flow fluctuation observable $v_0(p_T)$, which has been found to be more sensitive to bulk viscosity and comparatively insensitive to shear effects [23, 37–39]. The difference reflects the distinct physical information encoded in the two observables. While R_{pT} integrates momentum correlations over a broad p_T range and is therefore primarily governed by the overall coherence of event-by-event momentum shifts, making it particularly susceptible to shear-induced smoothing, $v_0(p_T)$ resolves the momentum-dependent redistribution of radial-flow fluctuations and is thus more directly influenced by bulk-viscous effects that modify the spectral shape.

Additional insight is provided by removing the hadronic afterburner (“no afterburner”) which produces opposite trends in the two centrality bins: R_{pT} decreases in mid-central collisions but increases in peripheral ones. This behavior reflects a competition between correlation buildup during the hadronic stage and multiplicity-driven dilution effects, whose relative importance changes with system size.

Among the variations considered, reducing the nucleon size from $w = 1.12$ fm to 0.8 fm (“smaller nucleon”) yields the largest and most robust enhancement of R_{pT} across both centralities, underscoring the strong sensitivity of the observable to initial-state granularity. A smaller nucleon width increases event-by-event fluctuations of local pressure gradients and hence amplifies fluctuations of the collective radial flow (β_T). At a schematic level, the correlated momentum shift induced by radial expansion can be expressed as $\delta p_T \sim m_T \delta \beta_T$,

so that the two-particle covariance scales parametrically as

$$C_m \sim \langle \delta p_T \delta p_T \rangle \sim \langle m_T^2 \rangle \langle \delta \beta_T^2 \rangle. \quad (3)$$

Reducing w enhances $\langle \delta \beta_T^2 \rangle$ by increasing the granularity of the initial conditions, thereby strengthening collective momentum correlations and leading to a larger R_{pT} .

Taken together, Fig. 2 demonstrates that R_{pT} is sensitive to multiple stages of the collision dynamics, including initial-state structure, viscous hydrodynamic evolution, and late-stage hadronic effects. The absence of a universal response pattern across centrality underscores that the observable probes competing fluctuation mechanisms whose relative contributions evolve with system size. Rather than a drawback, this feature makes R_{pT} a valuable complementary constraint on the modeling of event-by-event dynamics, particularly when combined with observables that primarily constrain average collective flow.

3.3. Impact of kinematic acceptance on the beam-energy dependence

In Fig. 1, we presented a baseline comparison between model calculations and STAR data at $\sqrt{s_{NN}} = 200$ GeV, using the experimental kinematic window $0.2 < p_T < 2$ GeV. As a consistency check, we also examined the sensitivity of the result to variations of the lower p_T cut within the model and found that modest changes of p_T^{\min} lead to visible shifts in the magnitude of the integrated fluctuation observable. This observation already indicates that, for p_T -integrated correlation measures, the numerical value does not solely reflect the underlying dynamics, but also depends on how the momentum-space correlation structure is projected onto a finite kinematic acceptance. This projection effect must therefore be carefully controlled when comparing results across different beam energies.

This motivates a more systematic examination of kinematic effects when comparing results across different beam energies. In experimental measurements, the commonly used acceptance windows are not identical: at RHIC, STAR typically employs $0.2 < p_T < 2$ GeV at $\sqrt{s_{NN}} = 200$ GeV [14], while at the LHC, ALICE uses $0.15 < p_T < 2$ GeV at $\sqrt{s_{NN}} = 2.76$ and 5.02 TeV [15, 16]. However, even if identical absolute p_T cuts were applied at all energies, the corresponding momentum window would not probe the same relative portion of the underlying particle spectrum. As the characteristic transverse momentum scale of the system increases with beam energy, and varies with centrality at fixed energy, the same fixed p_T range samples different regions of the soft momentum distribution and therefore different components of the underlying momentum correlations.

The physical origin of this effect can be understood from the structure of the single-particle transverse-momentum spectra themselves. For a fixed centrality class, we find that identified-particle p_T spectra at different beam energies approximately collapse onto a common curve when expressed in terms of the dimensionless variable $p_T/\langle p_T \rangle$, up to an overall normalization factor. This approximate scaling indicates that the ensemble-averaged mean transverse momentum $\langle p_T \rangle$ provides a natural

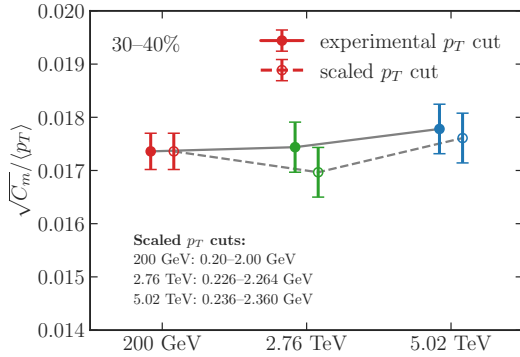


Figure 3: Beam-energy dependence of $\sqrt{C_m}/\langle p_T \rangle$ for charged hadrons in 30–40% central collisions, comparing results obtained with experimental kinematic cuts (solid symbols) and with scaled p_T cuts (open symbols). The experimental cut setup follows the published experimental acceptances: $0.2 < p_T < 2$ GeV at $\sqrt{s_{NN}} = 200$ GeV (STAR) and $0.15 < p_T < 2$ GeV at $\sqrt{s_{NN}} = 2.76$ and 5.02 TeV (ALICE). The scaled-cut results use energy-dependent windows defined relative to the charged-particle mean transverse momentum and anchored to the STAR acceptance at 200 GeV, yielding $0.226 < p_T < 2.264$ GeV at 2.76 TeV and $0.236 < p_T < 2.360$ GeV at 5.02 TeV.

soft momentum scale of the system. Consequently, a fixed absolute p_T window corresponds to different relative locations in scaled momentum space as the beam energy or centrality changes, even when the same nominal cuts are applied.

Guided by this observation, we introduce a “scaled-cut” prescription designed to align the kinematic acceptance relative to a common soft momentum scale when comparing different beam energies. To disentangle genuine beam-energy systematics from kinematic projection effects, Fig. 3 compares two setups for mid-central (30–40%) collisions. The first corresponds to the “experimental cut” setup, in which the published acceptance windows are used at each beam energy. The second employs a scaled acceptance defined as

$$p_T^{\min}(\sqrt{s_{NN}}) = \alpha \langle p_T \rangle_{\text{ch}}(\sqrt{s_{NN}}), \quad (4)$$

$$p_T^{\max}(\sqrt{s_{NN}}) = \beta \langle p_T \rangle_{\text{ch}}(\sqrt{s_{NN}}), \quad (5)$$

where $\langle p_T \rangle_{\text{ch}}$ is the charged-particle mean transverse momentum in the same centrality class. The constants α and β are fixed by anchoring the scaled window to the STAR acceptance at $\sqrt{s_{NN}} = 200$ GeV, $0.2 < p_T < 2$ GeV. This procedure yields energy-dependent momentum windows, $0.226 < p_T < 2.264$ GeV at 2.76 TeV and $0.236 < p_T < 2.360$ GeV at 5.02 TeV, that shift both the lower and upper edges upward at LHC energies, reflecting the harder underlying spectra.

Figure 3 shows that, under the experimental cuts, the integrated fluctuation measure exhibits an increase with beam energy. In contrast, when the scaled-cut prescription is applied, the results at both LHC energies are reduced relative to the fixed-cut case, with a larger suppression observed at $\sqrt{s_{NN}} = 2.76$ TeV. This behavior naturally follows from the shift of the scaled acceptance toward higher transverse momenta, which samples a harder region of the momentum distribution than the published experimental cuts.

The reduction of $\sqrt{C_m}/\langle p_T \rangle$ under the scaled-cut prescription is closely connected to the p_T -cut dependence discussed

in Sec. 3.1. There, lowering the minimum p_T cut enhanced the fluctuation signal by including a larger fraction of very soft particles, where collective radial dynamics are strongest. In the present case, the scaled cuts act in the opposite direction at LHC energies by increasing both p_T^{\min} and p_T^{\max} relative to the experimental acceptance, thereby suppressing contributions from the softest, most strongly correlated part of the spectrum.

Within current uncertainties, the resulting beam-energy dependence under scaled cuts may even appear non-monotonic. We emphasize, however, that this behavior should not be over-interpreted as evidence for a genuine non-monotonic dynamical trend. Rather, it reflects a general kinematic projection mechanism inherent to p_T -integrated fluctuation observables. Because R_{p_T} is dominated by correlations carried by the soft part of the spectrum, acceptance windows that shift toward higher relative momenta systematically suppress the measured fluctuation magnitude by reducing the weight of the most strongly correlated low- p_T particles. Scaled cuts make this suppression explicit by construction, while fixed absolute p_T cuts can induce it implicitly as the characteristic momentum scale of the system changes.

As a consequence, part of the observed beam-energy dependence of p_T -integrated fluctuation measures [14] may arise from kinematic projection effects rather than changes in the underlying correlation strength itself (see Appendix B). When fixed absolute p_T cuts are used across energies, the acceptance effectively drifts relative to the soft momentum scale of the system, altering the balance between soft and semi-soft contributions as the spectra harden or soften with $\sqrt{s_{NN}}$. The scaled-cut comparison presented here provides a controlled demonstration of this effect at top RHIC and LHC energies and highlights its direct relevance for RHIC Beam Energy Scan measurements [40–44], where the progressive softening of the single-particle spectra can significantly enhance acceptance-induced biases in the apparent beam-energy systematics.

3.4. Species dependence and effective kinematic projection

Identified-particle measurements provide a more differential probe of transverse-momentum fluctuations by isolating their dependence on hadron mass and species composition. They offer a direct test of whether the observed correlations exhibit the mass dependence expected from fluctuating radial flow and help clarify how changes in particle composition may influence inclusive fluctuation measurements. At present, such species-resolved measurements of transverse-momentum fluctuations are not available experimentally, and the results presented here should therefore be viewed as exploratory predictions within the calibrated framework.

Figure 4 shows the fluctuation observable $\sqrt{C_m}/\langle p_T \rangle$ evaluated separately for identified π^\pm , K^\pm , and p/\bar{p} in central (0–5%) Au+Au collisions at $\sqrt{s_{NN}} = 200$ GeV, using a common kinematic window $0.2 < p_T < 2$ GeV for all species. For reference, the corresponding result for inclusive charged hadrons in the same centrality and acceptance is also indicated. A clear mass ordering is observed: the fluctuation measure increases systematically from pions to kaons to protons. Since the mean transverse momentum itself grows with particle mass,

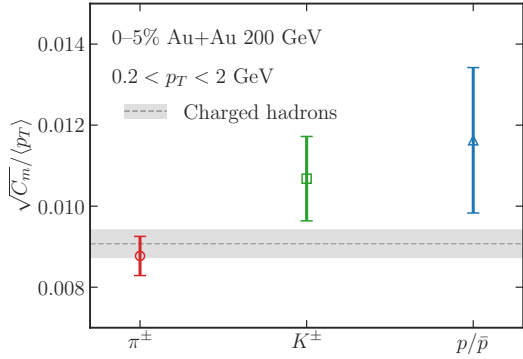


Figure 4: Species dependence of $\sqrt{C_m}/\langle p_T \rangle$ for identified π^\pm , K^\pm , and p/\bar{p} in central (0–5%) Au+Au collisions at $\sqrt{s_{NN}} = 200$ GeV, evaluated in a common kinematic window $0.2 < p_T < 2$ GeV. The shaded band and dashed line indicate the corresponding result for inclusive charged hadrons in the same centrality and acceptance.

$\langle p_T \rangle_p > \langle p_T \rangle_K > \langle p_T \rangle_\pi$, this ordering implies an even stronger mass dependence of the absolute covariance $\sqrt{C_m}$. In other words, heavier particles not only have larger mean momenta, but also exhibit substantially stronger event-by-event momentum correlations.

This behavior is naturally understood as a consequence of fluctuating radial flow. Event-wise variations of the collective transverse velocity field lead to momentum shifts, $\delta p_T \sim m_T \delta \beta_T$, that scale approximately with particle mass, such that heavier hadrons experience larger absolute responses to the same underlying flow fluctuation. As a result, the two-particle covariance C_m , which encodes correlated momentum fluctuations, is amplified for heavier species. The observed mass ordering therefore provides further evidence that the dominant contribution to the fluctuation observable originates from collective dynamics rather than from few-particle or non-collective sources.

Importantly, the species dependence observed in Fig. 4 is closely connected to the kinematic acceptance effects discussed in Secs. 3.1 and 3.3. Although the same absolute p_T window is applied to all species, this window corresponds to different regions of the underlying spectra when measured relative to each species’ characteristic momentum scale. Expressed in units of $p_T/\langle p_T \rangle$, the fixed window probes a softer and more flow-dominated region for protons than for pions, while sampling a comparatively harder region for lighter species. As a result, the fixed p_T cut does not merely reveal the intrinsic mass dependence of the fluctuations but systematically amplifies it by enhancing the relative weight of soft, strongly correlated particles for heavier hadrons. Consequently, different particle species effectively project different parts of the underlying momentum-correlation structure even under identical kinematic cuts.

From this perspective, the mass ordering seen here represents an internal analogue of the explicit p_T -cut dependence discussed earlier. Varying the particle species at fixed acceptance shifts the effective location of the kinematic window in scaled momentum space in much the same way as changing the lower or upper p_T cut for a single species. The enhanced sen-

sitivity of heavier hadrons to both collective flow fluctuations and kinematic acceptance effects further reinforces the interpretation that the measured transverse-momentum correlations are dominated by global, event-wise dynamics of the expanding medium.

4. Conclusions

In this work, we have presented a systematic model study of event-by-event transverse-momentum fluctuations in relativistic heavy-ion collisions, focusing on the observable $R_{p_T} \equiv \sqrt{C_m}/\langle p_T \rangle$ and its sensitivity to soft-sector dynamics and kinematic acceptance. Using a Bayesian-calibrated event-by-event hydrodynamic framework, we performed baseline comparisons to RHIC data, investigated controlled variations of model ingredients, and examined the interplay between dynamical and kinematic effects in beam-energy systematics.

At $\sqrt{s_{NN}} = 200$ GeV, the model reproduces the quantitative centrality dependence of the STAR measurements within the experimental acceptance. The remaining discrepancy in magnitude is traced to a pronounced sensitivity of R_{p_T} to the very soft part of the transverse-momentum spectrum, indicating that the integrated fluctuation signal is dominated by long-wavelength collective dynamics carried by low- p_T particles. This observation highlights the importance of kinematic acceptance in the interpretation of p_T -integrated fluctuation observables.

By varying individual model ingredients at fixed beam energy, we showed that R_{p_T} responds to multiple stages of the collision evolution, including initial-state granularity, viscous hydrodynamic damping, and late-stage hadronic rescattering. The magnitude and even the sign of these responses depend on centrality, underscoring that transverse-momentum fluctuations probe competing fluctuation mechanisms whose relative importance evolves with system size. This behavior demonstrates that R_{p_T} provides information complementary to average flow observables and offers an independent handle on event-by-event collective dynamics.

When comparing results across beam energies, we demonstrated that a substantial part of the apparent energy dependence of R_{p_T} obtained under fixed experimental p_T cuts can arise from kinematic projection effects. Introducing a scaled-cut prescription that aligns the acceptance relative to the characteristic soft momentum scale qualitatively modifies the observed energy dependence, emphasizing the need for acceptance-aware comparisons in RHIC-to-LHC studies and beam energy scan programs.

Finally, we explored the species dependence of transverse-momentum fluctuations in central Au+Au collisions at $\sqrt{s_{NN}} = 200$ GeV. A clear mass ordering is observed, with heavier hadrons exhibiting stronger momentum correlations. This behavior is naturally explained by fluctuating radial flow and provides an internal analogue of the p_T -cut dependence discussed earlier, illustrating how different particle species effectively probe different regions of the underlying momentum-correlation structure even within identical kinematic windows.

Taken together, our results establish transverse-momentum fluctuation observables as sensitive probes of collective dy-

namics whose quantitative interpretation requires careful control of kinematic acceptance and projection effects. Future experimental measurements that explore alternative p_T windows, identified-particle fluctuations, and differential extensions of the present analysis will provide valuable opportunities to further isolate dynamical contributions and to sharpen the sensitivity of p_T -correlation observables to the properties of the expanding quark-gluon plasma, in a manner complementary to traditional flow-based constraints.

Acknowledgements

The author acknowledges helpful discussions with workshop participants, especially I. Karpenko, R. Manikandhan and T. Reichert, at the workshop *The QCD Critical Point: Are We There Yet?* hosted by the Institute for Nuclear Theory (INT) at the University of Washington, which stimulated the present study. The author thanks the INT for its warm hospitality and stimulating research environment. This work was supported in part by the U.S. Department of Energy through the INT under Grant No. DE-FG02-00ER41132, and in part by the U.S. Department of Energy, Office of Science, Office of Nuclear Physics under Grant No. DE-AC02-05CH11231. Computational resources were provided by the Ohio Supercomputer Center [45]. The author acknowledges the use of ChatGPT for assistance with grammar refinement and clarity improvement during manuscript preparation.

Appendix A. Relation between the STAR and ALICE transverse-momentum fluctuation definitions

In Secs. 2.2 and 2.3, we introduced the transverse-momentum fluctuation observable $R_{p_T} = \sqrt{C_m}/\langle p_T \rangle$ and summarized the STAR and ALICE experimental prescriptions in a unified framework. In this appendix, we provide a compact analytical relation between the two definitions, clarifying why they yield nearly identical results in the present analysis.

For a given event k with multiplicity N_k , we denote the event-wise mean transverse momentum by $[p_T]_k = \frac{1}{N_k} \sum_i p_{T,i}$ and the ensemble-averaged mean by $\langle p_T \rangle = \langle [p_T]_k \rangle$. The STAR and ALICE definitions differ only in the choice of reference mean $p_{T,\text{ref}}$ entering the event-wise covariance (Eq. (1)):

$$p_{T,\text{ref}}^{\text{STAR}} = \langle p_T \rangle, \quad p_{T,\text{ref}}^{\text{ALICE}} = [p_T]_k.$$

Introducing the decomposition $p_{T,i} - \langle p_T \rangle = (p_{T,i} - [p_T]_k) + ([p_T]_k - \langle p_T \rangle)$, the STAR and ALICE single-event covariances, C_k^{STAR} and C_k^{ALICE} , are related by the exact identity

$$C_k^{\text{STAR}} = C_k^{\text{ALICE}} + ([p_T]_k - \langle p_T \rangle)^2. \quad (\text{A.1})$$

Here C_k denotes the event-wise covariance defined in Eq. (1), prior to the averaging over events that yields the experimentally reported quantity C_m . Averaging over events within a fixed centrality class yields

$$\langle C_k^{\text{STAR}} \rangle = \langle C_k^{\text{ALICE}} \rangle + \text{Var}([p_T]_k), \quad (\text{A.2})$$

where $\text{Var}([p_T]_k) \equiv \langle ([p_T]_k - \langle p_T \rangle)^2 \rangle$ is the event-by-event variance of the mean transverse momentum.

Equation (A.2) shows that the STAR definition contains, in addition to the ALICE-style two-particle covariance, an explicit contribution from fluctuations of the event-wise mean $[p_T]$ within the centrality bin. As discussed in Sec. 2.3, the magnitude of this additional term depends on the particle multiplicity and the width of the centrality selection.

In the present analysis, the use of relatively narrow centrality bins and the large multiplicities characteristic of RHIC and LHC collisions render $\text{Var}([p_T]_k)$ numerically small compared to the genuine two-particle correlation contribution. Consequently, the STAR and ALICE prescriptions yield nearly identical values of R_{p_T} when applied to the same set of model events with identical kinematic cuts, as explicitly demonstrated in Sec. 3.1. This near-equivalence justifies our use of a single representative definition in the presentation of results, while retaining both prescriptions as an internal consistency check on the robustness of the extracted fluctuation signal. However, in very peripheral collisions or for wide centrality selections, the variance term may become non-negligible.

Appendix B. Kinematic projection effects and beam-energy systematics at RHIC BES

The interpretation of the beam-energy dependence of the transverse-momentum fluctuation observable $R_{p_T} = \sqrt{C_m}/\langle p_T \rangle$ requires careful separation of genuine dynamical effects from kinematic projection effects associated with the finite p_T acceptance. This appendix provides a unified explanation of how fixed absolute p_T cuts affect both the magnitude and the apparent energy dependence of R_{p_T} at RHIC BES energies, and why a substantial part of the observed trend can arise from kinematics alone.

The two-particle covariance

$$C_m \sim \int dp_T dp'_T \left(\frac{dN}{dp_T} \right) \left(\frac{dN}{dp'_T} \right) \langle \delta p_T \delta p'_T \rangle \quad (\text{B.1})$$

is dominated by correlated momentum shifts generated by event-by-event fluctuations of collective radial expansion. To leading order, a fluctuation of the transverse flow velocity $\delta\beta_T$ induces a correlated shift of single-particle momenta, $\delta p_T \sim m_T \delta\beta_T$. Although higher- p_T particles experience larger absolute momentum shifts, the rapidly falling single-particle yield, dN/dp_T , suppresses their statistical weight. As a result, the dominant contribution to C_m arises from the low- p_T region, where particle production is largest. This feature underlies the strong sensitivity of C_m to the soft part of the spectrum.

At a fixed beam energy and centrality, modifying the p_T acceptance therefore has a direct and predictable effect on R_{p_T} . Extending the acceptance toward lower p_T includes additional particles from this correlation-dominated region, increasing the correlated covariance $\sqrt{C_m}$. At the same time, the ensemble-averaged mean transverse momentum $\langle p_T \rangle$ decreases due to the enhanced statistical weight of soft particles. Both effects act coherently to increase R_{p_T} . Conversely, restricting the acceptance

to higher p_T excludes soft correlated pairs, reduces $\sqrt{C_m}$, and increases $\langle p_T \rangle$, leading to a suppression of R_{p_T} . This behavior reflects a purely kinematic projection effect and does not imply any change in the underlying dynamics.

When a fixed absolute p_T window is applied across different beam energies in the RHIC BES, an additional effect enters. As the beam energy is lowered, the characteristic momentum scale of the system decreases, and the same fixed p_T window probes progressively harder regions of the spectrum when expressed in scaled units such as $p_T/\langle p_T \rangle$. This kinematic drift systematically removes the lowest- p_T particles that carry the largest share of the correlated covariance. As a result, $\sqrt{C_m}$ decreases with decreasing beam energy even if the intrinsic strength of collective fluctuations were unchanged.

The denominator $\langle p_T \rangle$ is affected in the opposite direction: excluding soft particles increases the measured mean transverse momentum. This increase acts in the same direction as the suppression of $\sqrt{C_m}$, further reducing R_{p_T} ; however, its quantitative impact is subleading compared to the loss of correlated soft pairs in the covariance. The correlated covariance C_m is a two-particle quantity dominated by the multiplicity-rich soft sector, whereas $\langle p_T \rangle$ is a single-particle moment that varies more smoothly with acceptance. Consequently, the suppression of $\sqrt{C_m}$ dominates, and the net effect is a decrease of R_{p_T} as the beam energy is lowered.

Across the wide energy range of the RHIC BES, this kinematic drift becomes pronounced. The fixed absolute p_T cut moves rapidly toward the tail of the spectrum at lower energies, leading to a substantial loss of soft, collectively correlated particles. The resulting kinematic suppression of R_{p_T} can therefore amplify the apparent beam-energy dependence observed in experimental measurements. Importantly, this mechanism operates independently of any genuine change in the microscopic fluctuation dynamics and must be accounted for when interpreting energy-dependent trends of p_T -integrated fluctuation observables.

Taken together, these considerations demonstrate that the decrease of R_{p_T} toward lower RHIC BES energies obtained with fixed absolute p_T cuts contains a significant kinematic component. A robust interpretation of beam-energy systematics therefore requires careful control of acceptance effects, either through scaled-cut prescriptions or through complementary differential measurements that explicitly resolve the momentum dependence of the underlying correlations.

References

- [1] J.-Y. Ollitrault, Anisotropy as a signature of transverse collective flow, *Phys. Rev. D* 46 (1992) 229–245. [doi:10.1103/PhysRevD.46.229](https://doi.org/10.1103/PhysRevD.46.229).
- [2] U. Heinz, R. Snellings, Collective flow and viscosity in relativistic heavy-ion collisions, *Ann. Rev. Nucl. Part. Sci.* 63 (2013) 123–151. [arXiv:1301.2826](https://arxiv.org/abs/1301.2826), [doi:10.1146/annurev-nucl-102212-170540](https://doi.org/10.1146/annurev-nucl-102212-170540).
- [3] S. A. Voloshin, A. M. Poskanzer, R. Snellings, Collective phenomena in non-central nuclear collisions, *Landolt-Bornstein* 23 (2010) 293–333. [arXiv:0809.2949](https://arxiv.org/abs/0809.2949), [doi:10.1007/978-3-642-01539-7_10](https://doi.org/10.1007/978-3-642-01539-7_10).
- [4] H. Song, S. A. Bass, U. Heinz, T. Hirano, C. Shen, 200 A GeV Au+Au collisions serve a nearly perfect quark-gluon liquid, *Phys. Rev. Lett.* 106 (2011) 192301, [Erratum: *Phys. Rev. Lett.* 109, 139904 (2012)]. [arXiv:1011.2783](https://arxiv.org/abs/1011.2783), [doi:10.1103/PhysRevLett.106.192301](https://doi.org/10.1103/PhysRevLett.106.192301).
- [5] J. E. Bernhard, J. S. Moreland, S. A. Bass, Bayesian estimation of the specific shear and bulk viscosity of quark-gluon plasma, *Nature Phys.* 15 (11) (2019) 1113–1117. [doi:10.1038/s41567-019-0611-8](https://doi.org/10.1038/s41567-019-0611-8).
- [6] G. Nijs, W. van der Schee, U. Gürsoy, R. Snellings, Transverse Momentum Differential Global Analysis of Heavy-Ion Collisions, *Phys. Rev. Lett.* 126 (20) (2021) 202301. [arXiv:2010.15130](https://arxiv.org/abs/2010.15130), [doi:10.1103/PhysRevLett.126.202301](https://doi.org/10.1103/PhysRevLett.126.202301).
- [7] G. Nijs, W. van der Schee, U. Gürsoy, R. Snellings, Bayesian analysis of heavy ion collisions with the heavy ion computational framework Trajectum, *Phys. Rev. C* 103 (5) (2021) 054909. [arXiv:2010.15134](https://arxiv.org/abs/2010.15134), [doi:10.1103/PhysRevC.103.054909](https://doi.org/10.1103/PhysRevC.103.054909).
- [8] D. Everett, et al., Phenomenological constraints on the transport properties of QCD matter with data-driven model averaging, *Phys. Rev. Lett.* 126 (24) (2021) 242301. [arXiv:2010.03928](https://arxiv.org/abs/2010.03928), [doi:10.1103/PhysRevLett.126.242301](https://doi.org/10.1103/PhysRevLett.126.242301).
- [9] D. Everett, et al., Multisystem Bayesian constraints on the transport coefficients of QCD matter, *Phys. Rev. C* 103 (5) (2021) 054904. [arXiv:2011.01430](https://arxiv.org/abs/2011.01430), [doi:10.1103/PhysRevC.103.054904](https://doi.org/10.1103/PhysRevC.103.054904).
- [10] S. Jeon, V. Koch, Event by event fluctuations, 2004, pp. 430–490. [arXiv:hep-ph/0304012](https://arxiv.org/abs/hep-ph/0304012), [doi:10.1142/9789812795533_0007](https://doi.org/10.1142/9789812795533_0007).
- [11] S. Gavin, M. Abdel-Aziz, Measuring Shear Viscosity Using Transverse Momentum Correlations in Relativistic Nuclear Collisions, *Phys. Rev. Lett.* 97 (2006) 162302. [arXiv:nucl-th/0606061](https://arxiv.org/abs/nucl-th/0606061), [doi:10.1103/PhysRevLett.97.162302](https://doi.org/10.1103/PhysRevLett.97.162302).
- [12] D. Adamova, et al., Event by event fluctuations of the mean transverse momentum in 40, 80 and 158 A GeV / c Pb - Au collisions, *Nucl. Phys. A* 727 (2003) 97–119. [arXiv:nucl-ex/0305002](https://arxiv.org/abs/nucl-ex/0305002), [doi:10.1016/j.nuclphysa.2003.07.018](https://doi.org/10.1016/j.nuclphysa.2003.07.018).
- [13] J. Adams, et al., Incident energy dependence of pt correlations at RHIC, *Phys. Rev. C* 72 (2005) 044902. [arXiv:nucl-ex/0504031](https://arxiv.org/abs/nucl-ex/0504031), [doi:10.1103/PhysRevC.72.044902](https://doi.org/10.1103/PhysRevC.72.044902).
- [14] J. Adam, et al., Collision-energy dependence of p_t correlations in Au + Au collisions at energies available at the BNL Relativistic Heavy Ion Collider, *Phys. Rev. C* 99 (4) (2019) 044918. [arXiv:1901.00837](https://arxiv.org/abs/1901.00837), [doi:10.1103/PhysRevC.99.044918](https://doi.org/10.1103/PhysRevC.99.044918).
- [15] B. Abelev, et al., Event-by-event mean p_T fluctuations in pp and Pb-Pb collisions at the LHC, *Eur. Phys. J. C* 74 (10) (2014) 3077. [arXiv:1407.5530](https://arxiv.org/abs/1407.5530), [doi:10.1140/epjc/s10052-014-3077-y](https://doi.org/10.1140/epjc/s10052-014-3077-y).
- [16] S. Acharya, et al., System size and energy dependence of the mean transverse momentum fluctuations at the LHC, *Eur. Phys. J. C* 85 (7) (2025) 776. [arXiv:2411.09334](https://arxiv.org/abs/2411.09334), [doi:10.1140/epjc/s10052-025-14325-4](https://doi.org/10.1140/epjc/s10052-025-14325-4).
- [17] G. Aad, et al., Disentangling Sources of Momentum Fluctuations in Xe+Xe and Pb+Pb Collisions with the ATLAS Detector, *Phys. Rev. Lett.* 133 (25) (2024) 252301. [arXiv:2407.06413](https://arxiv.org/abs/2407.06413), [doi:10.1103/PhysRevLett.133.252301](https://doi.org/10.1103/PhysRevLett.133.252301).
- [18] S. Gavin, Traces of thermalization from transverse momentum fluctuations in nuclear collisions, *Phys. Rev. Lett.* 92 (2004) 162301. [arXiv:nucl-th/0308067](https://arxiv.org/abs/nucl-th/0308067), [doi:10.1103/PhysRevLett.92.162301](https://doi.org/10.1103/PhysRevLett.92.162301).
- [19] S. Gavin, L. McLerran, G. Moschelli, Long Range Correlations and the Soft Ridge in Relativistic Nuclear Collisions, *Phys. Rev. C* 79 (2009) 051902. [arXiv:0806.4718](https://arxiv.org/abs/0806.4718), [doi:10.1103/PhysRevC.79.051902](https://doi.org/10.1103/PhysRevC.79.051902).
- [20] P. Bozek, Transverse-momentum-flow correlations in relativistic heavy-ion collisions, *Phys. Rev. C* 93 (4) (2016) 044908. [arXiv:1601.04513](https://arxiv.org/abs/1601.04513), [doi:10.1103/PhysRevC.93.044908](https://doi.org/10.1103/PhysRevC.93.044908).
- [21] J.-F. Paquet, Applications of emulation and Bayesian methods in heavy-ion physics, *J. Phys. G* 51 (10) (2024) 103001. [arXiv:2310.17618](https://arxiv.org/abs/2310.17618), [doi:10.1088/1361-6471/ad6a2b](https://doi.org/10.1088/1361-6471/ad6a2b).
- [22] D. Everett, et al., Role of bulk viscosity in deuteron production in ultrarelativistic nuclear collisions, *Phys. Rev. C* 106 (6) (2022) 064901. [arXiv:2203.08286](https://arxiv.org/abs/2203.08286), [doi:10.1103/PhysRevC.106.064901](https://doi.org/10.1103/PhysRevC.106.064901).
- [23] L. Du, Characterizing radial flow fluctuations in relativistic heavy-ion collisions at top RHIC and LHC energies [arXiv:2508.07184](https://arxiv.org/abs/2508.07184).
- [24] J. H. Putschke, et al., The JETSCAPE framework [arXiv:1903.07706](https://arxiv.org/abs/1903.07706).
- [25] J. S. Moreland, J. E. Bernhard, S. A. Bass, Alternative ansatz to wounded nucleon and binary collision scaling in high-energy nuclear collisions, *Phys. Rev. C* 92 (1) (2015) 011901. [arXiv:1412.4708](https://arxiv.org/abs/1412.4708), [doi:10.1103/PhysRevC.92.011901](https://doi.org/10.1103/PhysRevC.92.011901).
- [26] W. Broniowski, W. Florkowski, M. Chojnacki, A. Kisiel, Free-streaming approximation in early dynamics of relativistic heavy-ion collisions, *Phys. Rev. C* 80 (2009) 034902. [arXiv:0812.3393](https://arxiv.org/abs/0812.3393), [doi:10.1103/PhysRevC.80.034902](https://doi.org/10.1103/PhysRevC.80.034902).

[PhysRevC.80.034902](#).

[27] J. Liu, C. Shen, U. Heinz, Pre-equilibrium evolution effects on heavy-ion collision observables, *Phys. Rev. C* 91 (6) (2015) 064906, [Erratum: *Phys. Rev. C* 92, 049904 (2015)]. [arXiv:1504.02160](#), [doi:10.1103/PhysRevC.91.064906](#).

[28] B. Schenke, S. Jeon, C. Gale, (3+1)D hydrodynamic simulation of relativistic heavy-ion collisions, *Phys. Rev. C* 82 (2010) 014903. [arXiv:1004.1408](#), [doi:10.1103/PhysRevC.82.014903](#).

[29] B. Schenke, S. Jeon, C. Gale, Higher flow harmonics from (3+1)D event-by-event viscous hydrodynamics, *Phys. Rev. C* 85 (2012) 024901. [arXiv:1109.6289](#), [doi:10.1103/PhysRevC.85.024901](#).

[30] J.-F. Paquet, C. Shen, G. S. Denicol, M. Luzum, B. Schenke, S. Jeon, C. Gale, Production of photons in relativistic heavy-ion collisions, *Phys. Rev. C* 93 (4) (2016) 044906. [arXiv:1509.06738](#), [doi:10.1103/PhysRevC.93.044906](#).

[31] F. Cooper, G. Frye, Comment on the Single Particle Distribution in the Hydrodynamic and Statistical Thermodynamic Models of Multiparticle Production, *Phys. Rev. D* 10 (1974) 186. [doi:10.1103/PhysRevD.10.186](#).

[32] C. Shen, Z. Qiu, H. Song, J. Bernhard, S. Bass, U. Heinz, The iEBE-VISHNU code package for relativistic heavy-ion collisions, *Comput. Phys. Commun.* 199 (2016) 61–85. [arXiv:1409.8164](#), [doi:10.1016/j.cpc.2015.08.039](#).

[33] M. McNeilis, D. Everett, U. Heinz, Particilization in fluid dynamical simulations of heavy-ion collisions: The iS3D module, *Comput. Phys. Commun.* 258 (2021) 107604. [arXiv:1912.08271](#), [doi:10.1016/j.cpc.2020.107604](#).

[34] J. Weil, et al., Particle production and equilibrium properties within a new hadron transport approach for heavy-ion collisions, *Phys. Rev. C* 94 (5) (2016) 054905. [arXiv:1606.06642](#), [doi:10.1103/PhysRevC.94.054905](#).

[35] S. A. Voloshin, Mean $p(t)$ fluctuations from two particle and four particle correlations [arXiv:nucl-th/0206052](#).

[36] S. A. Voloshin, Transverse radial expansion in nuclear collisions and two particle correlations, *Phys. Lett. B* 632 (2006) 490–494. [arXiv:nucl-th/0312065](#), [doi:10.1016/j.physletb.2005.11.024](#).

[37] T. Parida, R. Samanta, J.-Y. Ollitrault, Probing collectivity in heavy-ion collisions with fluctuations of the pT spectrum, *Phys. Lett. B* 857 (2024) 138985. [arXiv:2407.17313](#), [doi:10.1016/j.physletb.2024.138985](#).

[38] S. Acharya, et al., Long-range transverse momentum correlations and radial flow in Pb–Pb collisions at the LHC [arXiv:2504.04796](#).

[39] G. Aad, et al., Evidence for the collective nature of radial flow in Pb+Pb collisions with the ATLAS detector [arXiv:2503.24125](#).

[40] B. I. Abelev, et al., Systematic Measurements of Identified Particle Spectra in pp, d^+ Au and Au+Au Collisions from STAR, *Phys. Rev. C* 79 (2009) 034909. [arXiv:0808.2041](#), [doi:10.1103/PhysRevC.79.034909](#).

[41] L. Adamczyk, et al., Bulk Properties of the Medium Produced in Relativistic Heavy-Ion Collisions from the Beam Energy Scan Program, *Phys. Rev. C* 96 (4) (2017) 044904. [arXiv:1701.07065](#), [doi:10.1103/PhysRevC.96.044904](#).

[42] A. Bzdak, S. Esumi, V. Koch, J. Liao, M. Stephanov, N. Xu, Mapping the Phases of Quantum Chromodynamics with Beam Energy Scan, *Phys. Rept.* 853 (2020) 1–87. [arXiv:1906.00936](#), [doi:10.1016/j.physrep.2020.01.005](#).

[43] L. Du, Bulk medium properties of heavy-ion collisions from the beam energy scan with a multistage hydrodynamic model, *Phys. Rev. C* 110 (1) (2024) 014904. [arXiv:2401.00596](#), [doi:10.1103/PhysRevC.110.014904](#).

[44] L. Du, A. Sorensen, M. Stephanov, The QCD phase diagram and Beam Energy Scan physics: A theory overview, *Int. J. Mod. Phys. E* 33 (07) (2024) 2430008. [arXiv:2402.10183](#), [doi:10.1142/9789811294679_0007](#).

[45] Ohio Supercomputer Center (1987).
URL <http://osc.edu/ark:/19495/f5s1ph73>